

Expansion of the high field-boosted superconductivity in UTe_2 under pressure

Sheng Ran^{1,2,3}, Shanta R. Saha^{1,2}, I-Lin Liu^{1,2}, David
Graf⁴, Johnpierre Paglione^{1,2}, Nicholas P. Butch^{1,2*}

¹ *Maryland Quantum Materials Center,
Department of Physics,
University of Maryland,
College Park, MD 20742, USA*

² *NIST Center for Neutron Research,
National Institute of Standards and Technology,
Gaithersburg, MD 20899, USA*

³ *Department of Physics,
Washington University in St. Louis,
St. Louis, MO 63130, USA*

⁴ *National High Magnetic Field Laboratory,
Florida State University,
Tallahassee, FL 32313, USA*

* *email: nbutch@umd.edu*

(Dated: July 8, 2021)

Abstract

Magnetic field induced superconductivity is a fascinating quantum phenomenon, whose origin is yet to be fully understood. The recently discovered spin triplet superconductor, UTe_2 , exhibits two such superconducting phases, with the second one reentering in the magnetic field of 45 T and persisting up to 65 T. More surprisingly, in order to induce this superconducting phase, the magnetic field has to be applied in a special angle range, not along any high symmetry crystalline direction. Here we investigated the evolution of this high-field induced superconducting phase under pressure. Two superconducting phases merges together under pressure, and the zero resistance persists up to 45 T, the field limit of the current study. We also reveal that the high field-induced superconducting phase is completely decoupled from the first order field polarized phase transition, different from previously known example of field induced superconductivity in URhGe , indicating a superconductivity boosted by a different paring mechanism.

INTRODUCTION

The recent evidence for spin triplet superconductivity in UTe_2 has opened an avenue for the study of topological superconductivity¹. The superconducting state of UTe_2 closely resembles that of ferromagnetic superconductors, but the normal state is paramagnetic and shows no indication of magnetic ordering²⁻⁴. Spin triplet pairing is strongly indicated by the extremely large, anisotropic upper critical field H_{c2} ^{1,5}, nodes on the superconducting gap^{6,7}, and the temperature independent NMR Knight shift in the superconducting state^{8,9}. The superconducting order parameter comprises two components and breaks time reversal symmetry^{10,11}. A nontrivial topology is suggested by the observation of chiral in-gap bound states by scanning tunneling spectroscopy¹².

Even more striking, UTe_2 hosts two independent field-induced superconducting phases¹³⁻¹⁶, with the higher-field phase reentering at a high magnetic field of 45 T and persisting up to 65 T when the magnetic field is aligned over a limited angular range about the normal direction of the (011) plane. The quasi-two-dimensional Fermi surface revealed by band structure calculations and photoemission measurements¹⁷⁻¹⁹, as well as the lack of a ferromagnetic ground state, has led to suggestions that the field-induced superconductivity in UTe_2 is due to reduced dimensionality instead of magnetic fluctuations^{20,21}: a magnetic field applied parallel to quasi 2D conducting layers will stabilize superconductivity when the magnetic energy reaches the hopping amplitude between the conducting layers^{20,22}.

In this work we investigate the evolution of the magnetic field-induced superconducting phases in UTe_2 as pressure is applied to samples oriented specifically along the off-axis angle which stabilizes the high-field phase. Over a range of pressures near 1 GPa, the two different superconducting phases merge together, and the electrical resistance remains zero up to at least 45 T, a remarkably large value for a superconductor with a 3 K critical temperature. The high field-induced superconducting phase is completely decoupled from the first-order transition to a field-polarized state, suggesting that magnetic fluctuations may not be crucial to this reentrant superconductivity. At pressures exceeding the critical pressure at which metamagnetic phase transition extrapolates to zero magnetic field, we observe features with the same temperature dependence as the high field-induced superconducting phase, further investigation of which might shed light on the mechanism reentrant superconductivity.

RESULTS AND DISCUSSION

Pressure-magnetic field phase diagram

To characterize the evolution of the high field-induced superconducting phase under pressure, we performed complementary measurements of electrical resistance R and tunnel diode oscillator (TDO) frequency Δf , which is sensitive to the change of both electrical resistance and magnetic susceptibility. Two samples were studied for which the magnetic field was applied approximately 25 degrees and 30 degrees, respectively, away from the b axis towards c . At ambient pressure, three distinct phases were observed as shown in Fig. 1: a field polarized state FP with greatly enhanced magnetization and resistance^{13,15,16,23}; the low field superconducting phase, SC_{PM} , coexisting with the paramagnetic state; and the high field-induced superconducting phase, SC_{FP} , existing inside the field polarized state. Criterion used to infer critical magnetic field for each phase are explained in the Supplementary Information (See Supplementary Figure 4-7).

Absent in this field configuration is another field induced superconducting phase that is observed on the low-field side of the metamagnetic field H_{FP} when magnetic field is applied along the b axis. For magnetic field along the b axis, applied pressure suppresses the metamagnetic field to zero at 1.5 GPa and forces a phase transition inside the paramagnetic state at a crossover pressure P_x , from SC_{PM1} to SC_{PM2} , in zero magnetic field at approximately 1 GPa²⁴. Recent symmetry analysis indicates that the SC_{PM1} phase has two-component order parameter while order parameter of SC_{PM2} phase only has one component¹¹. Our measurements in this study do not exhibit any field-induced features²⁴, so we infer that the SC_{PM1} - SC_{PM2} boundary is nearly vertical in the $H - P$ plane. At pressures exceeding 1.5 GPa, long range magnetic order is stabilized²⁵⁻²⁸, whose features have been interpreted in terms of both ferromagnetism^{24,25} and antiferromagnetism²⁷. Without an unambiguous experimental proof of the nature of this phase, in this study we label it as a magnetically ordered phase, M.

The pressure-magnetic field phase diagram for the magnetic field in this angle range is summarized in Fig. 1b. All three phases manifest clear evolution under pressure, as seen in R and Δf in Fig. 2. The metamagnetic field is monotonically suppressed by the applied pressure, similar to the behavior for field along b ²⁴, although it starts at a higher value. The

metamagnetic field vanishes at a critical pressure P_c between 1.47 and 1.54 GPa, giving rise to a spontaneous polarized state in zero magnetic field beyond this pressure. Over the entire pressure range, both R and Δf change discontinuously on passing through the metamagnetic field in the normal state, implying that it maintains the first-order metamagnetic transition observed at ambient pressure^{15,23,29}.

Upon initial increase of the pressure, the stability of the both superconducting phases is enhanced: the upper critical field of SC_{PM} , H_{c2} , increases and the critical onset field of SC_{FP} , H_1 , which coincides with the metamagnetic field, decreases. In an intermediate crossover pressure range, the phase boundary between SC_{PM} and SC_{FP} is no longer visible in the electrical resistance; this remains zero up to 45 T at base temperature, which is noteworthy as it is the largest DC magnetic field currently available to experiment (Fig. 3b). As the pressure further increases, the upper critical field of SC_{PM} is limited by the metamagnetic field and decreases, but the critical onset field of SC_{FP} starts to increase, and the two superconducting phases are no longer connected. When the metamagnetic field vanishes, SC_{PM} is suppressed completely.

Subtle differences between the electrical resistance and TDO samples highlight the effects of their slight angular offset (Fig. 2). As the TDO sample sits at a slightly larger angle away from the b axis, the upper critical field of SC_{PM} has a smaller value and critical onset field of SC_{FP} has a larger value at ambient pressure. The SC_{PM} and SC_{FP} phases remain connected over a much smaller pressure range. Similarly, the field polarized state starts above a higher magnetic field because the metamagnetic field is larger, but it is suppressed faster upon increasing pressure, and vanishes also at P_c .

The discontinuous nature of the metamagnetic transition at H_{FP} is conspicuous in the resistance data. At low pressures (Fig. 3c), a sharp upward jump marking the FP phase boundary is replaced at low temperatures by a sharp downward jump marking the SC_{FP} phase boundary. An additional hallmark of first-order transitions, namely field-hysteresis is also readily apparent (inset of Fig. 3c). In the intermediate pressure range, H_{FP} limits the lower-field superconducting phase SC_{PM} (Fig. 3d). Here, the transitions associated with H_{FP} are again hysteretic (inset of Fig. 3d). Interestingly, the decoupled SC_{FP} phase appears to also exhibit some small hysteresis, the origin of which may be associated with details of the field-reentrance. These features are consistent at all measured pressures (Fig. 3a, b).

These details reveal important points about the relationships between the many electronic

phases. The low- and high-field superconducting phases always exist on opposite sides of the metamagnetic transition H_{FP} , upon which Fermi surface reconstruction has been suggested based on thermoelectric power and Hall effect measurements^{23,30,31}. In addition, in the low pressure range, SC_{FP} only appears on the high-field side of the metamagnetic field (Fig. 2a, b), while SC_{PM} only exists at fields lower than the metamagnetic field. The role of the metamagnetic field switches in the intermediate pressure range, where the metamagnetic field truncates the low-field phase SC_{PM} . This behavior is apparent in both panels of Fig. 2c, where the high-temperature part of the upper critical field of SC_{PM} curve rises rapidly as temperature decreases, extrapolating to field values far higher than the metamagnetic field, but then, as soon as the upper critical field of SC_{PM} coincides with the metamagnetic field, the behavior suddenly changes and the upper critical field of SC_{PM} becomes almost temperature independent down to low temperatures. Taken together, these facts imply that the SC_{PM} and SC_{FP} phases separated by the metamagnetic transition might have different superconducting pairing that are unique to PM and FP, respectively. It is particularly striking that both low- and high-field superconducting phases look like they would cover much larger ranges of field were they not limited by the metamagnetic field.

In the high pressure range, the critical onset field of SC_{FP} and the metamagnetic field are well separated, by more than 20 T. This is crucial for the understanding of the pairing mechanism of the SC_{FP} phase. In the case of URhGe, the reentrance of superconductivity can be explained in terms of ferromagnetic fluctuations parallel to the direction of the magnetic field. In that case, reentrant SC occurs in the vicinity of the magnetic critical field. In UTe₂ at low pressure, the SC_{FP} phase resembles somewhat the reentrant phase in URhGe, leading to the speculation that magnetic fluctuations are also responsible for reentrant superconductivity in UTe₂. However, here we show clearly that the SC_{FP} phases can exist in the region far away from the field polarized phase line, indicating a possibility scenario that magnetic fluctuations are not responsible for the pairing mechanism. Future experiments to investigate magnetic fluctuations in the vicinity of the SC_{FP} phase at pressure above 1.3 GPa will potential shed light on the pairing mechanism.

Anomaly in the high-pressure region

A striking characteristic of the high-pressure FP phase is the emergence of additional features in the field range between the M and SC_{FP} phases. These anomalies, denoted A_{FP}, are pronounced in the Δf data, and noticeable in R data (Fig. 4). It is not clear whether these anomalies correspond to a thermodynamically distinct phase. In order to trace the evolution of these anomalies, we introduced a criteria to define the boundaries as shown in the Supplementary Materials. These anomalies exhibit a clear temperature dependence below 1.2 K. This notable similarity to the temperature dependence of SC_{FP} suggests that A_{FP} is a closely related phenomenon, with a similar energy scale to that of the superconductivity. This distinguishes A_{FP} from the zero-field magnetically ordered phase M, which has a higher-temperature ordering temperature relative to superconductivity, that continues to increase with applied pressure.

An exciting possibility is that A_{FP} is a precursor to superconductivity. Previous theoretical studies have shown that in extreme magnetic field Landau levels will have dramatic influence on the low-temperature behavior of the upper critical field^{32–34}. Indeed, a more recent theoretical study indicates that SC_{FP} might be a form of superconductivity that is enhanced by high-field Landau quantization of the conduction electrons³⁵. Therefore, A_{FP} and SC_{FP} may actually be the same superconducting phase occurring at different Landau levels, analogous to Shubnikov-de Haas oscillations. A challenge to this interpretation is that A_{FP} is not accompanied by a zero resistance state (Fig. 3a), but a plausible explanation for this is that A_{FP} is actually partially superconducting due to the effects of energy-level broadening are stronger at lower field. Based on the inverse-field periodicity of A_{FP}, the next Landau level will be centered at approximately 100 T, achieving zero resistance at magnetic fields as low as 90 T, which is practically achievable using the strongest available non-destructive pulsed magnet systems.

METHODS

Crystal synthesis

Single crystals of UTe₂ were synthesized by the chemical vapor transport method using iodine as the transport agent. Elements of U and Te with atomic ratio 2:3 were sealed

in an evacuated quartz tube, together with 3 mg/cm³ iodine. The ampoule was gradually heated up and hold in the temperature gradient of 1060/1000 °C for 7 days, after which it was furnace cooled to room temperature. The crystal structure was determined by *x*-ray powder diffraction using a Rigaku *x*-ray diffractometer with Cu-K_α radiation. Crystal orientation was determined by Laue *x*-ray diffraction performed with a Photonic Science *x*-ray measurement system.

Measurement

Magnetoresistance and tunnel diode oscillator (TDO) measurements were performed at the National High Magnetic Field Laboratory, Tallahassee, using the 45-T hybrid magnet. A non-magnetic piston-cylinder pressure cell was used for measurements under pressure up to 1.57 GPa, with Daphne oil 7575 as the pressure medium. Pressure was calibrated at low temperatures by measuring the fluorescence wavelength of ruby, which has a known temperature and pressure dependence. The TDO technique uses an *LC* oscillator circuit biased by a tunnel diode whose resonant frequency is determined by the values of *LC* components, with the inductance *L* given by a coil that contains the sample under study; the change of its electrical resistance and magnetic properties results in a change in resonant frequency. Identification of commercial equipment does not imply recommendation or endorsement by NIST. Error bars correspond to an uncertainty of one standard deviation.

DATA AVAILABILITY

The data that support the findings of this study are available from the corresponding author upon reasonable request.

ACKNOWLEDGMENTS

We acknowledge D. Agterberg, G. S. Boebinger, A. E. Koshelev, A. Lebed, and V. P. Mineev for inspiring discussions. Research at the University of Maryland was supported by the National Institute of Standards and Technology (NIST), the US National Science Foundation (NSF) Division of Materials Research Award No. DMR-1610349, the US Department of

Energy (DOE) Award No. DE-SC-0019154 (experimental investigations), and the Gordon and Betty Moore Foundation’s EPiQS Initiative through Grant No. GBMF4419 (materials synthesis). Work performed at the National High Magnetic Field Laboratory, USA (NHMFL) was supported by NSF through NSF/DMR-1644779 and the State of Florida.

AUTHOR CONTRIBUTIONS

N. Butch and S. Ran conceived and designed the study. S. Ran and S. R. Saha synthesized the single crystalline samples. S. Ran, S. R. Saha, I. Liu and D. Graf performed the electrical resistivity and tunnel diode oscillator measurements. S.R., J.P. and N.P.B. analyzed the data and wrote the paper with everyone’s contribution.

COMPETING INTERESTS

The authors declare no competing interests.

-
- ¹ Ran, S. *et al.* Nearly ferromagnetic spin-triplet superconductivity. *Science* **365**, 684–687 (2019).
- ² Sundar, S. *et al.* Coexistence of ferromagnetic fluctuations and superconductivity in the actinide superconductor UTe₂. *Phys. Rev. B* **100**, 140502 (2019). URL <https://link.aps.org/doi/10.1103/PhysRevB.100.140502>.
- ³ Hutanu, V. *et al.* Low-temperature crystal structure of the unconventional spin-triplet superconductor UTe₂ from single-crystal neutron diffraction. *Acta Crystallographica Section B* **76**, 137–143 (2020). URL <https://doi.org/10.1107/S2052520619016950>.
- ⁴ Duan, C. *et al.* Incommensurate spin fluctuations in the spin-triplet superconductor candidate UTe₂. *Phys. Rev. Lett.* **125**, 237003 (2020). URL <https://link.aps.org/doi/10.1103/PhysRevLett.125.237003>.
- ⁵ Aoki, D. *et al.* Unconventional superconductivity in heavy fermion UTe₂. *J. Phys. Soc. Jpn.* **88**, 043702 (2019). URL <https://doi.org/10.7566/JPSJ.88.043702>.
- ⁶ Metz, T. *et al.* Point-node gap structure of the spin-triplet superconductor UTe₂. *Phys. Rev. B* **100**, 220504 (2019). URL <https://link.aps.org/doi/10.1103/PhysRevB.100.220504>.

- ⁷ Bae, S. *et al.* Anomalous normal fluid response in a chiral superconductor UTe₂. *Nature Communications* **12**, 2644 (2021). URL <https://doi.org/10.1038/s41467-021-22906-6>.
- ⁸ Nakamine, G. *et al.* Superconducting properties of heavy fermion UTe₂ revealed by ¹²⁵Te-nuclear magnetic resonance. *J. Phys. Soc. Jpn.* **88**, 113703 (2020). URL <https://doi.org/10.7566/JPSJ.88.113703>.
- ⁹ Nakamine, G. *et al.* Anisotropic response of spin susceptibility in the superconducting state of UTe₂ probed with ¹²⁵Te-NMR measurement. *Phys. Rev. B* **103**, L100503 (2021). URL <https://link.aps.org/doi/10.1103/PhysRevB.103.L100503>.
- ¹⁰ Hayes, I. M. *et al.* Weyl superconductivity in UTe₂. *Preprint at: arXiv 2002.02539* (2020).
- ¹¹ Shishidou, T., Suh, H. G., Brydon, P. M. R., Weinert, M. & Agterberg, D. F. Topological band and superconductivity in UTe₂. *Phys. Rev. B* **103**, 104504 (2021). URL <https://link.aps.org/doi/10.1103/PhysRevB.103.104504>.
- ¹² Jiao, L. *et al.* Chiral superconductivity in heavy-fermion metal UTe₂. *Nature* **579**, 523–527 (2020). URL <https://doi.org/10.1038/s41586-020-2122-2>.
- ¹³ Ran, S. *et al.* Extreme magnetic field-boosted superconductivity. *Nature Physics* **15**, 1250–1254 (2019). URL <https://doi.org/10.1038/s41567-019-0670-x>.
- ¹⁴ Knebel, G. *et al.* Field-reentrant superconductivity close to a metamagnetic transition in the heavy-fermion superconductor UTe₂. *J. Phys. Soc. Jpn.* **88**, 063707 (2019). URL <https://doi.org/10.7566/JPSJ.88.063707>.
- ¹⁵ Knafo, W. *et al.* Magnetic-field-induced phenomena in the paramagnetic superconductor UTe₂. *J. Phys. Soc. Jpn.* **88**, 063705 (2019). URL <https://doi.org/10.7566/JPSJ.88.063705>.
- ¹⁶ Knafo, W. *et al.* Comparison of two superconducting phases induced by a magnetic field in UTe₂. *Communications Physics* **4**, 40 (2021). URL <https://doi.org/10.1038/s42005-021-00545-z>.
- ¹⁷ Miao, L. *et al.* Low energy band structure and symmetries of UTe₂ from angle-resolved photoemission spectroscopy. *Phys. Rev. Lett.* **124**, 076401 (2020). URL <https://link.aps.org/doi/10.1103/PhysRevLett.124.076401>.
- ¹⁸ Xu, Y., Sheng, Y. & Yang, Y.-f. Quasi-two-dimensional fermi surfaces and unitary spin-triplet pairing in the heavy fermion superconductor UTe₂. *Phys. Rev. Lett.* **123**, 217002 (2019). URL <https://link.aps.org/doi/10.1103/PhysRevLett.123.217002>.

- ¹⁹ Ishizuka, J., Sumita, S., Daido, A. & Yanase, Y. Insulator-metal transition and topological superconductivity in UTe_2 from a first-principles calculation. *Phys. Rev. Lett.* **123**, 217001 (2019). URL <https://link.aps.org/doi/10.1103/PhysRevLett.123.217001>.
- ²⁰ Lebed, A. G. & Yamaji, K. Restoration of superconductivity in high parallel magnetic fields in layered superconductors. *Phys. Rev. Lett.* **80**, 2697–2700 (1998). URL <https://link.aps.org/doi/10.1103/PhysRevLett.80.2697>.
- ²¹ Mineev, V. P. Reentrant superconductivity in UTe_2 . *JETP Letters* (2020). URL <https://doi.org/10.1134/S0021364020120036>.
- ²² Lebed, A. G. Restoration of superconductivity in high magnetic fields in UTe_2 . *Mod. Phys. Lett. B* **34**, 2030007 (2021). URL <https://doi.org/10.1142/S0217984920300070>.
- ²³ Miyake, A. *et al.* Metamagnetic transition in heavy fermion superconductor UTe_2 . *J. Phys. Soc. Jpn.* **88**, 063706 (2019). URL <https://doi.org/10.7566/JPSJ.88.063706>.
- ²⁴ Lin, W.-C. *et al.* Tuning magnetic confinement of spin-triplet superconductivity. *npj Quantum Materials* **5**, 68 (2020). URL <https://doi.org/10.1038/s41535-020-00270-w>.
- ²⁵ Ran, S. *et al.* Enhancement and reentrance of spin triplet superconductivity in UTe_2 under pressure. *Phys. Rev. B* **101**, 140503 (2020). URL <https://link.aps.org/doi/10.1103/PhysRevB.101.140503>.
- ²⁶ Braithwaite, D. *et al.* Multiple superconducting phases in a nearly ferromagnetic system. *Communications Physics* **2**, 147 (2019). URL <https://doi.org/10.1038/s42005-019-0248-z>.
- ²⁷ Thomas, S. M. *et al.* Evidence for a pressure-induced antiferromagnetic quantum critical point in intermediate-valence UTe_2 . *Sci Adv* **6**, eabc8709 (2020). URL <http://advances.sciencemag.org/content/6/42/eabc8709.abstract>.
- ²⁸ Aoki, D. *et al.* Multiple superconducting phases and unusual enhancement of the upper critical field in UTe_2 . *J. Phys. Soc. Jpn.* **89**, 053705 (2021). URL <https://doi.org/10.7566/JPSJ.89.053705>.
- ²⁹ Imajo, S. *et al.* Thermodynamic investigation of metamagnetism in pulsed high magnetic fields on heavy fermion superconductor UTe_2 . *J. Phys. Soc. Jpn.* **88**, 083705 (2019). URL <https://doi.org/10.7566/JPSJ.88.083705>.
- ³⁰ Niu, Q. *et al.* Fermi-surface instability in the heavy-fermion superconductor UTe_2 . *Phys. Rev. Lett.* **124**, 086601 (2020). URL <https://link.aps.org/doi/10.1103/PhysRevLett.124.086601>.

- ³¹ Niu, Q. *et al.* Evidence of fermi surface reconstruction at the metamagnetic transition of the strongly correlated superconductor UTe₂. *Phys. Rev. Research* **2**, 033179 (2020). URL <https://link.aps.org/doi/10.1103/PhysRevResearch.2.033179>.
- ³² Gruenberg, L. W. & Gunther, L. Effect of orbital quantization on the critical field of type-ii superconductors. *Phys. Rev.* **176**, 606–613 (1968). URL <https://link.aps.org/doi/10.1103/PhysRev.176.606>.
- ³³ Tešanović, Z., Rasolt, M. & Xing, L. Quantum limit of a flux lattice: Superconductivity and magnetic field in a new relationship. *Phys. Rev. Lett.* **63**, 2425–2428 (1989). URL <https://link.aps.org/doi/10.1103/PhysRevLett.63.2425>.
- ³⁴ Song, K. W. & Koshelev, A. E. Strong landau-quantization effects in high-magnetic-field superconductivity of a two-dimensional multiple-band metal near the lifshitz transition. *Phys. Rev. B* **95**, 174503 (2017). URL <https://link.aps.org/doi/10.1103/PhysRevB.95.174503>.
- ³⁵ Park, M. J., Kim, Y. B. & Lee, S. Geometric superconductivity in 3d hofstadter butterfly. *Preprint at: arXiv:2007.16205* (2020).

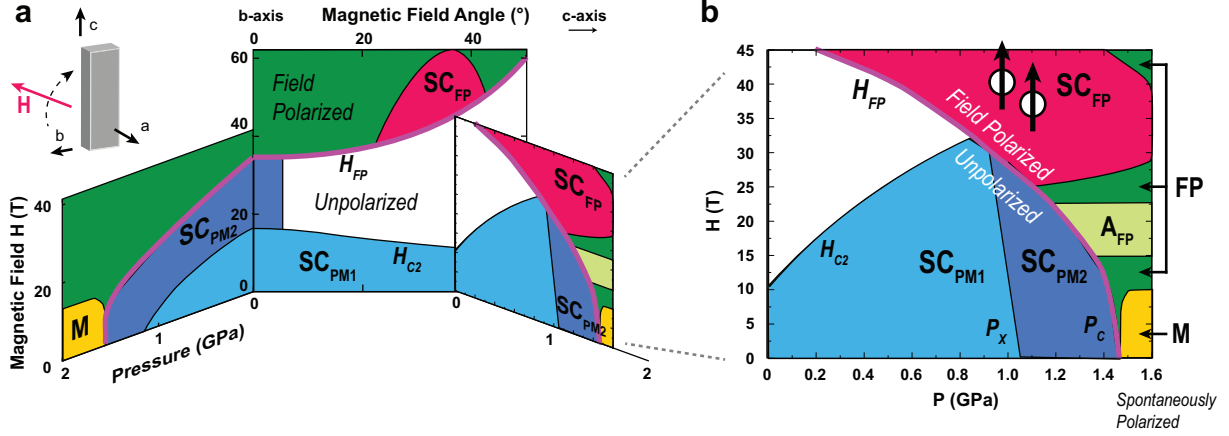


FIG. 1. The stability of superconducting and magnetic phases of UTe₂ as a function of magnetic field strength and angle, and applied pressure. a) The zero-field superconducting phase SC_{PM1} exhibits a strongly direction dependent upper critical field H_{C2} . Along the crystallographic b -axis, the reentrant superconducting phase SC_{PM2} is stabilized up to a first-order magnetic transition at H_{FP} , above which exists a magnetically polarized phase FP. Applied pressure uniformly suppresses all field scales and H_{FP} bounds superconductivity up to a critical pressure P_c . b) For a magnetic field oriented between 25 and 30 degrees between the b - and c -axes, the high-field reentrant superconductivity SC_{FP} stabilizes in the FP phase. Applied pressure enhances SC_{PM1}, which meets a decreasing H_{FP} at a crossover region P_x . Here, SC_{PM1} transitions to SC_{PM2}, which survives up to P_c , where it is replaced by magnetic order M. Below P_x , H_{FP} is a lower bound on SC_{FP}, but above P_x , the two are decoupled and SC_{FP} survives beyond P_c . An anomaly A_{FP}, suggestive of Landau-level superconductivity, emerges above P_c . The phase diagram is based on the resistance data shown in Fig. 2.

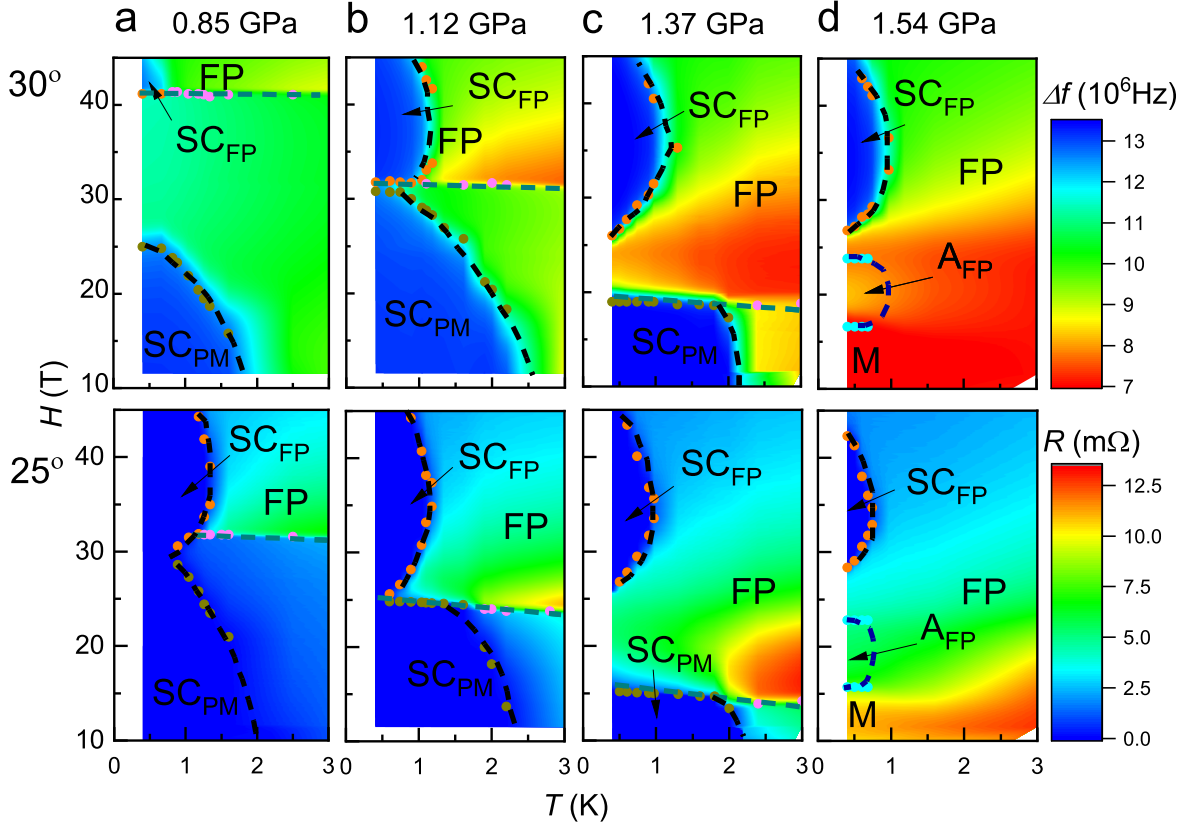


FIG. 2. **High-field tunnel diode oscillator (TDO) frequency (top row) and resistance (bottom row) at different pressures.** TDO frequency is sensitive to the change of both electrical resistance and magnetic susceptibility of the sample. Magnetic field is applied at 30 degree from b axis towards c axis for TDO measurement, and 25 degree from b axis towards c axis for resistance measurement. a) In the low-pressure region, H_{FP} serves as a lower bound to SC_{FP} , whose dome is cut off discontinuously. b) At crossover pressures P_x , H_{FP} falls approximately between SC_{FP} and SC_{PM} , whose ranges of stability would otherwise overlap. c) Above P_x , H_{FP} serves as the upper field limit for SC_{PM} . d) Above P_c , long-range ordered magnetism M sets in while SC_{FP} survives and the anomalous feature A_{FP} emerges as a local maximum in Δf . Solid dots are from experimental data, dashed lines are guide for the eye. Note that TDO and resistance measurements are performed for slightly different magnetic field direction, which leads to the slight different phase diagrams for each pressure.

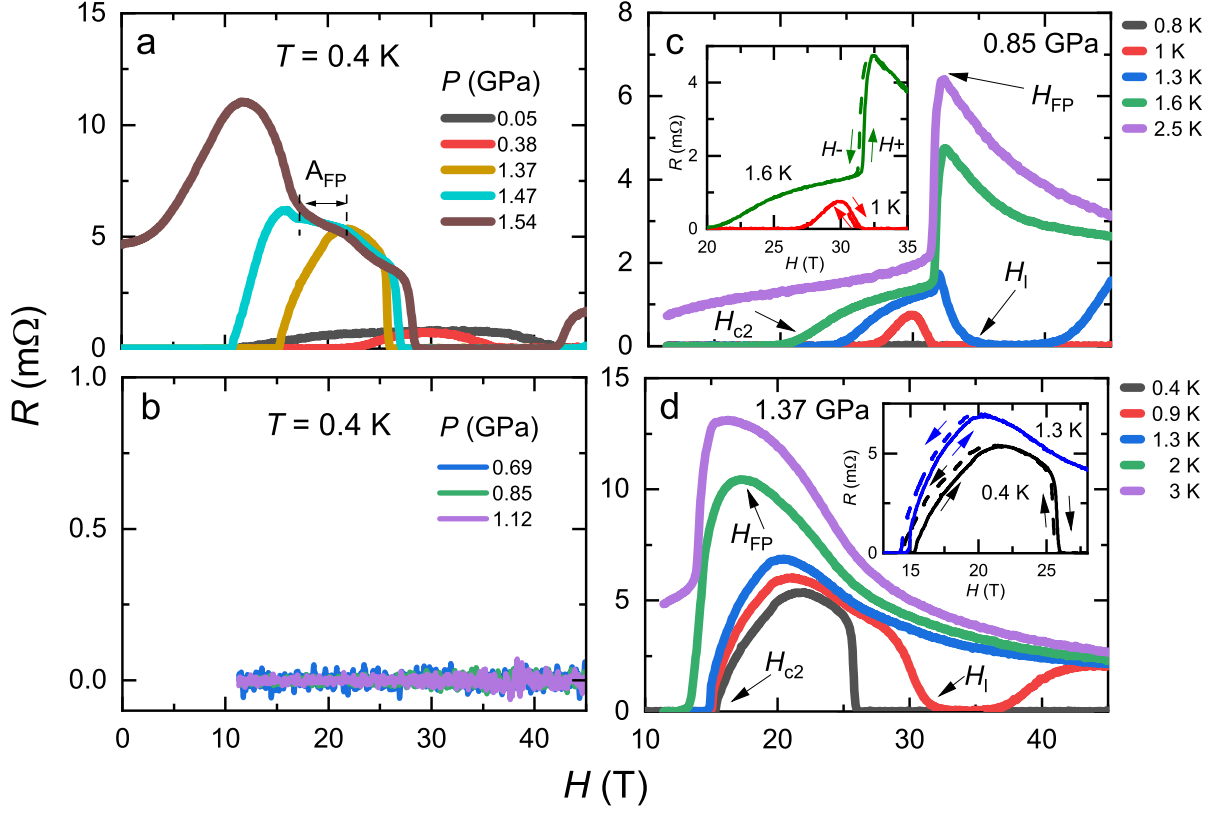


FIG. 3. **High-field magnetoresistance, highlighting different phase boundaries at different pressures.** Magnetic field is applied at 25 degree from b axis towards c axis. a) Pressure-dependence of 0.4 K magnetoresistance, showing the sharpening of phase boundaries at higher pressures and emergence of high-pressure phase A_{FP} . b) The resistance at pressures 0.69, 0.85, and 1.12 GPa is zero between 11 T and 45 T at 0.4 K. Zero resistance persists to zero magnetic field at these pressure values. c) For fields lower than H_{FP} , the superconducting transitions H_{C2} are broad, but H_{FP} is sharp. As shown in inset, H_{FP} is hysteretic, reflecting the 1st order transition, both at high temperatures in the FP phase and low temperature in the SC_{FP} phase. d) Much sharper superconducting phase boundaries occur once H_{FP} limits SC_{FP} . As shown in inset, low-field phase boundaries are hysteretic and first order, as is the onset of SC_{FP} .

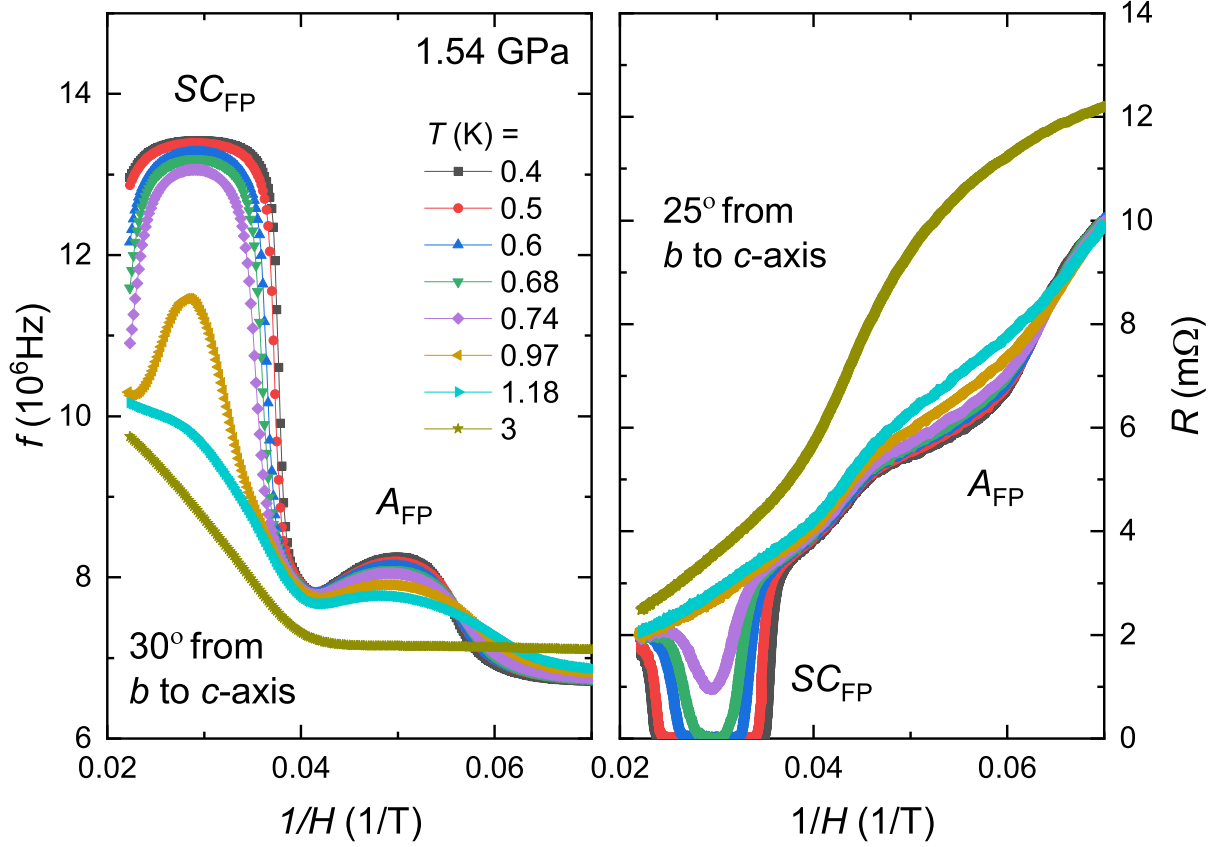


FIG. 4. **Additional anomalies emerge in the high pressure region.** A_{FP} phase appears at 1.54 GPa in both TDO and resistance data, which have the same temperature dependence as SC_{FP} phase, indicating A_{FP} phase might be the precursor of superconductivity. Magnetic field is applied at 30 degree from b axis towards c axis for TDO measurement, and 25 degree from b axis towards c axis for resistance measurement.